AEDC-TR-86-18

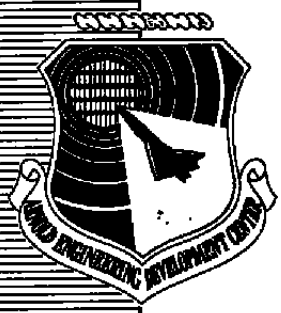

An Evaluation of Nozzle Afterbody Code - ARO2P

Frederick C. Guyton
Calspan Corporation/AEDC Division

July 1986

Final Report for Period November 1, 1981 – December 1, 1985

ARNOLD ENGINEERING DEVELOPMENT CENTER
ARNOLD AIR FORCE STATION, TENNESSEE
AIR FORCE SYSTEMS COMMAND
UNITED STATES AIR FORCE

NOTICES

When U. S. Government drawings, specifications, or other data are used for any purpose other than a definitely related Government procurement operation, the Government thereby incurs no responsibility nor any obligation whatsoever, and the fact that the Government may have formulated, furnished, or in any way supplied the said drawings, specifications, or other data, is not to be regarded by implication or otherwise, or in any manner licensing the holder or any other person or corporation, or conveying any rights or permission to manufacture, use, or sell any patented invention that may in any way be related thereto.

Qualified users may obtain copies of this report from the Defense Technical Information Center.

References to named commercial products in this report are not to be considered in any sense as an endorsement of the product by the United States Air Force or the Government.

This report has been reviewed by the Office of Public Affairs (PA) and is releasable to the National Technical Information Service (NTIS). At NTIS, it will be available to the general public, including foreign nations.

APPROVAL STATEMENT

This report has been reviewed and approved.

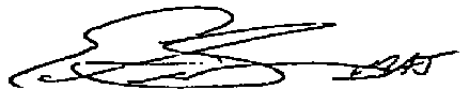

MALCOLM E. GIVINS, Major, CF
Facility Technology Division
Directorate of Technology
Deputy for Operations

Approved for publication:

FOR THE COMMANDER

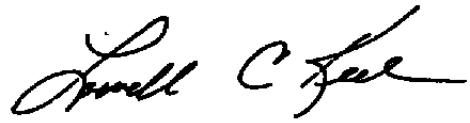

LOWELL C. KEEL, Lt Colonel, USAF
Director of Technology
Deputy for Operations

UNCLASSIFIED

SECURITY CLASSIFICATION OF THIS PAGE

REPORT DOCUMENTATION PAGE

1a. REPORT SECURITY CLASSIFICATION UNCLASSIFIED	1b. RESTRICTIVE MARKINGS
2a. SECURITY CLASSIFICATION AUTHORITY	3. DISTRIBUTION/AVAILABILITY OF REPORT Approved for public release; distribution unlimited.
2b. DECLASSIFICATION/DOWNGRADING SCHEDULE	
4. PERFORMING ORGANIZATION REPORT NUMBER(S) AEDC-TR-86-18	5. MONITORING ORGANIZATION REPORT NUMBER(S)
6a. NAME OF PERFORMING ORGANIZATION Arnold Engineering Development Center 6b. OFFICE SYMBOL (If applicable) DOF	7a. NAME OF MONITORING ORGANIZATION
6c. ADDRESS (City, State and ZIP Code) Air Force Systems Command Arnold Air Force Station, TN 37389 -5000	7b. ADDRESS (City, State and ZIP Code)
8a. NAME OF FUNDING/SPONSORING ORGANIZATION Arnold Engineering Development Center 8b. OFFICE SYMBOL (If applicable) DOT	9. PROCUREMENT INSTRUMENT IDENTIFICATION NUMBER
8c. ADDRESS (City, State and ZIP Code) Air Force Systems Command Arnold Air Force Station, TN 37389 -5000	10. SOURCE OF FUNDING NOS. PROGRAM ELEMENT NO. 65807F; PROJECT NO DA04; TASK NO.; WORK UNIT NO
11. TITLE (Include Security Classification) See reverse side of this page.	
12. PERSONAL AUTHOR(S) Guyton, Frederick C., Calspan Corporation/AEDC Division	
13a. TYPE OF REPORT Final 13b. TIME COVERED FROM 11/1/81 TO 12/1/85	14. DATE OF REPORT (Yr., Mo., Day) July 1986 15. PAGE COUNT 35
16. SUPPLEMENTARY NOTATION Available in Defense Technical Information Center (DTIC).	

17 COSATI CODES			18. SUBJECT TERMS (Continue on reverse if necessary and identify by block number)
FIELD	GROUP	SUB GR.	computational fluid dynamics nozzle afterbody analysis
20	04		

19. ABSTRACT (Continue on reverse if necessary and identify by block number)

A project was undertaken to develop a computational fluid dynamics (CFD) code for use in nozzle afterbody analysis. Objectives were to create a three-dimensional code capable of calculating afterbody flows with accuracy quantitatively close to the Navier-Stokes solutions, but which would use significantly fewer computer resources. The resulting program coupled an inverse boundary-layer routine with an Euler code and incorporated a jet plume. Calculations were made for the axisymmetric AGARD 15-deg boattail afterbody with variations in nozzle pressure ratio for Mach numbers 0.6 and 0.9, and compared with experimental results. The code predicted drag changes with NPR which showed the proper variations, but the code did not provide the accuracy required for typical nozzle afterbody analysis.

20. DISTRIBUTION/AVAILABILITY OF ABSTRACT UNCLASSIFIED/UNLIMITED ☐ SAME AS RPT. ☒ DTIC USERS ☐	21. ABSTRACT SECURITY CLASSIFICATION UNCLASSIFIED
22a. NAME OF RESPONSIBLE INDIVIDUAL W. O. Cole	22b TELEPHONE NUMBER (Include Area Code) (615) 454-7813 22c OFFICE SYMBOL DOS

DD FORM 1473, 83 APR EDITION OF 1 JAN 73 IS OBSOLETE.

UNCLASSIFIED

SECURITY CLASSIFICATION OF THIS PAGE

Block 11: An Evaluation of Nozzle Afterbody Code-ARO2P

PREFACE

The work reported herein was conducted by the Arnold Engineering Development Center (AEDC), Air Force Systems Command (AFSC), at the request of the Arnold Engineering Development Center (AEDC/DOT). The AEDC/DOT project manager was Dr. Keith Kushman. The results were obtained by Calspan Corporation/AEDC Division, operating contractor for the aerospace flight dynamics testing effort at the AEDC, AFSC, Arnold Air Force Station, Tennessee. Analysis of the results was completed December 1, 1985. The effort was conducted under Air Force Project Number DA04PW. The manuscript was submitted for publication on March 28, 1986.

CONTENTS

ILLUSTRATIONS

Figure | Page

1.0 INTRODUCTION

The nozzle afterbody flow field is a complex interaction between a jet exhaust plume, the local free-stream flow, and the model afterbody surfaces. Variables that affect the afterbody flow field are nozzle geometry, afterbody geometry, nozzle afterbody base, exhaust jet temperature, exhaust jet gas constant, exhaust jet specific heat ratio, and nozzle pressure ratio (NPR). Other considerations are model scale, support system interference, downstream hardware interference, and free-stream effects such as Mach number, Reynolds number, and humidity. Much work has been performed at AEDC directed toward understanding these effects and manipulating them in a controlled environment to correctly simulate flight conditions in the wind tunnel. Kennedy in Ref. 1 summarized AEDC's work in this area up to the year 1980. Later investigations are reported by Price and Lucas in Refs. 2 and 3, respectively. With the increase in capabilities of mainframe computers, computational fluid dynamics (CFD) presents the opportunity to develop a tool for flow analysis complementary to the wind tunnel. Accurate flow simulation by CFD methods can provide details that are difficult, if not impossible, to obtain in wind tunnels. Information such as flow field velocity vectors and pressure contours in addition to typical wind tunnel data such as model surface pressure distributions and forces can be obtained from numerical solutions. Long-term objectives are for CFD to vastly decrease the requirements for nozzle afterbody wind tunnel testing through numerical simulation; however, presently, computer size and computational cost are limiting factors.

It was demonstrated by Jacocks, Peters, and Guyton in Ref. 4 that CFD can be a valuable tool for use on the nozzle afterbody problem. In this work, an axisymmetric, Navier-Stokes code (Ref. 5) was used to calculate the flow about the AGARD 15-deg boattail afterbody with a full flowing jet. The solutions generated were compared to wind tunnel test data. Figures 1 and 2 show details of the model used to obtain the experimental data (Ref. 6) and Fig. 3 shows a single plane view of the axisymmetric computational mesh. Unlike the computational model, the experimental article had a finite nozzle base thickness for instrumentation purposes. Shown in Fig. 4 is a comparison of the measured and computed pressure distributions over the afterbody at Mach 0.9 and design NPR. The two results agree well, except in the recompression region where the predicted results indicate a higher presure than was measured at the end of the afterbody. This difference may be attributed to the fact that there was no model base present in the numerical solution. Figure 5 presents a comparison of experimental and computational pressure drag versus NPR. The shape and magnitude of the variations are similar. The computations correctly predict that with pressure ratio increasing from the jet-off condition, an initial decrease in drag occurs, followed by an increase in drag to a maximum jet-on "peak drag" value. This region is characterized by an overexpanded jet plume and is referred to as the "drag bucket." Further increases in NPR cause a continuing

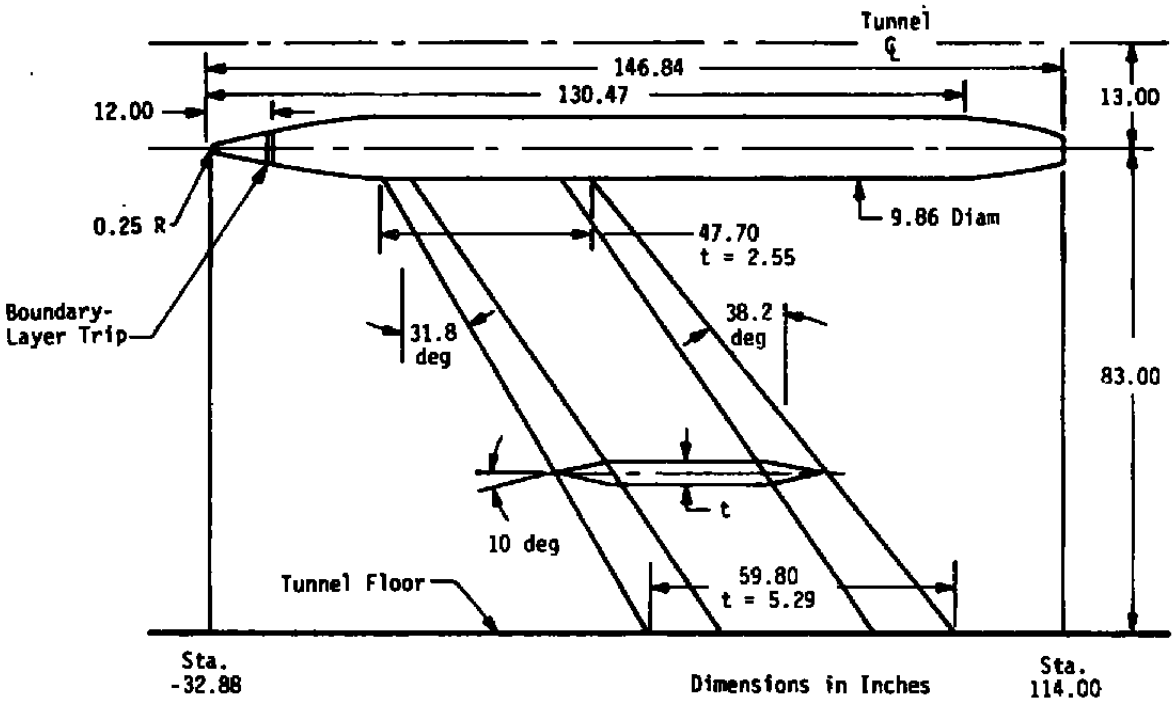

Figure 1. Axisymmetric model dimensions and location in tunnel 16T.

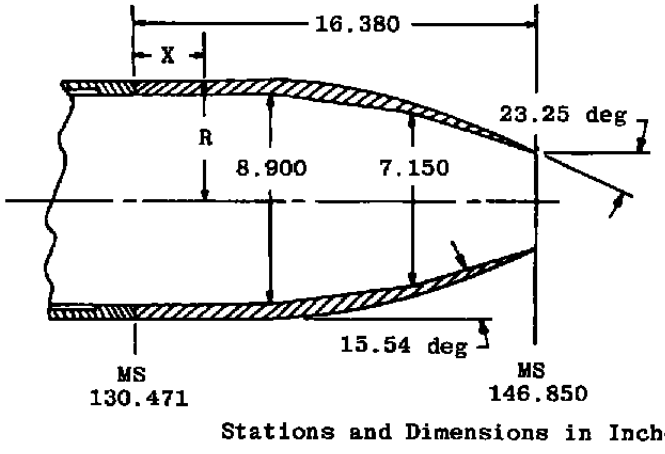

X	R	X	R
0	4.930	11.322	3.977
6.146	4.930	11.569	3.903
6.392	4.920	11.815	3.826
6.639	4.908	12.062	3.747
6.895	4.884	12.308	3.666
7.132	4.859	12.555	3.579
7.378	4.829	12.801	3.495
7.625	4.795	13.048	3.410
7.871	4.760	13.204	3.321
8.118	4.721	13.541	3.229
8.364	4.677	13.787	3.125
8.611	4.629	14.034	3.043
8.857	4.580	14.280	2.946
9.103	4.531	14.527	2.848
9.350	4.479	14.773	2.749
9.597	4.427	15.020	2.641
9.843	4.373	15.266	2.532
10.090	4.313	15.513	2.423
10.336	4.252	15.759	2.315
10.583	4.189	16.006	2.214
10.830	4.120	16.252	2.125
11.076	4.050	16.380	2.084

Figure 2. Afterbody contour and surface coordinates for axisymmetric model.

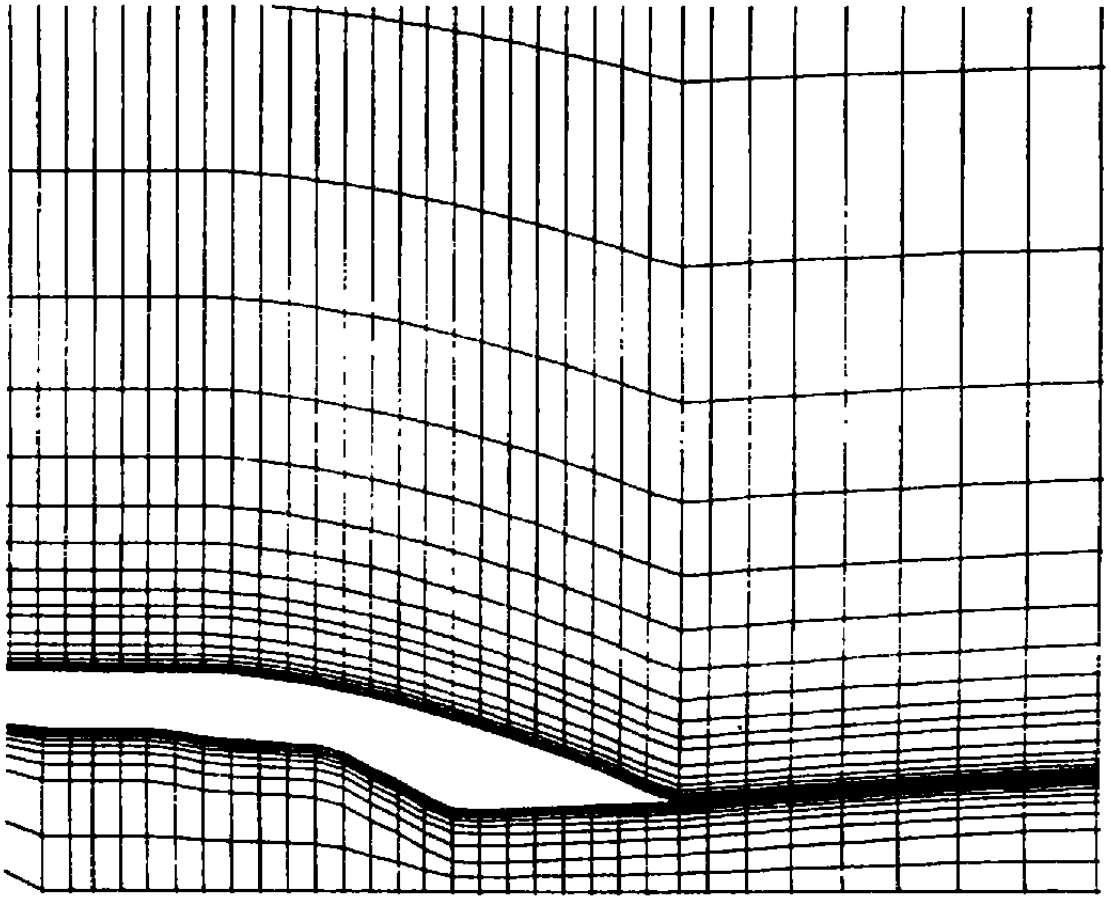

Figure 3. Nozzle afterbody computational mesh for axisymmetric Navier-Stokes calculations.

decrease in drag produced by the increasing blockage of the underexpanded jet plume. The computed values of drag coefficient are higher than experiment in the overexpanded jet regime; however, computational results correctly predict drag coefficient values at underexpanded jet conditions. The disagreement in the "drag bucket" region may also be attributable to no base being present in the computations, causing a larger influence of jet entrainment on the afterbody that was actually experienced. Figure 6 presents Mach number contour plots from the Navier-Stokes computations. The effects of increasing pressure ratio are easily observed in the plume Mach number contours; however, the effects causing variation in the integrated drag presented in Fig. 5 are not as evident when the afterbody region is viewed.

The effects of nozzle geometry, jet temperature, and Mach number were also investigated computationally by Jacocks, et al. The axisymmetric, Navier-Stokes code provided accuracy comparable to the previous nozzle pressure ratio analysis for these variables as well. In general,

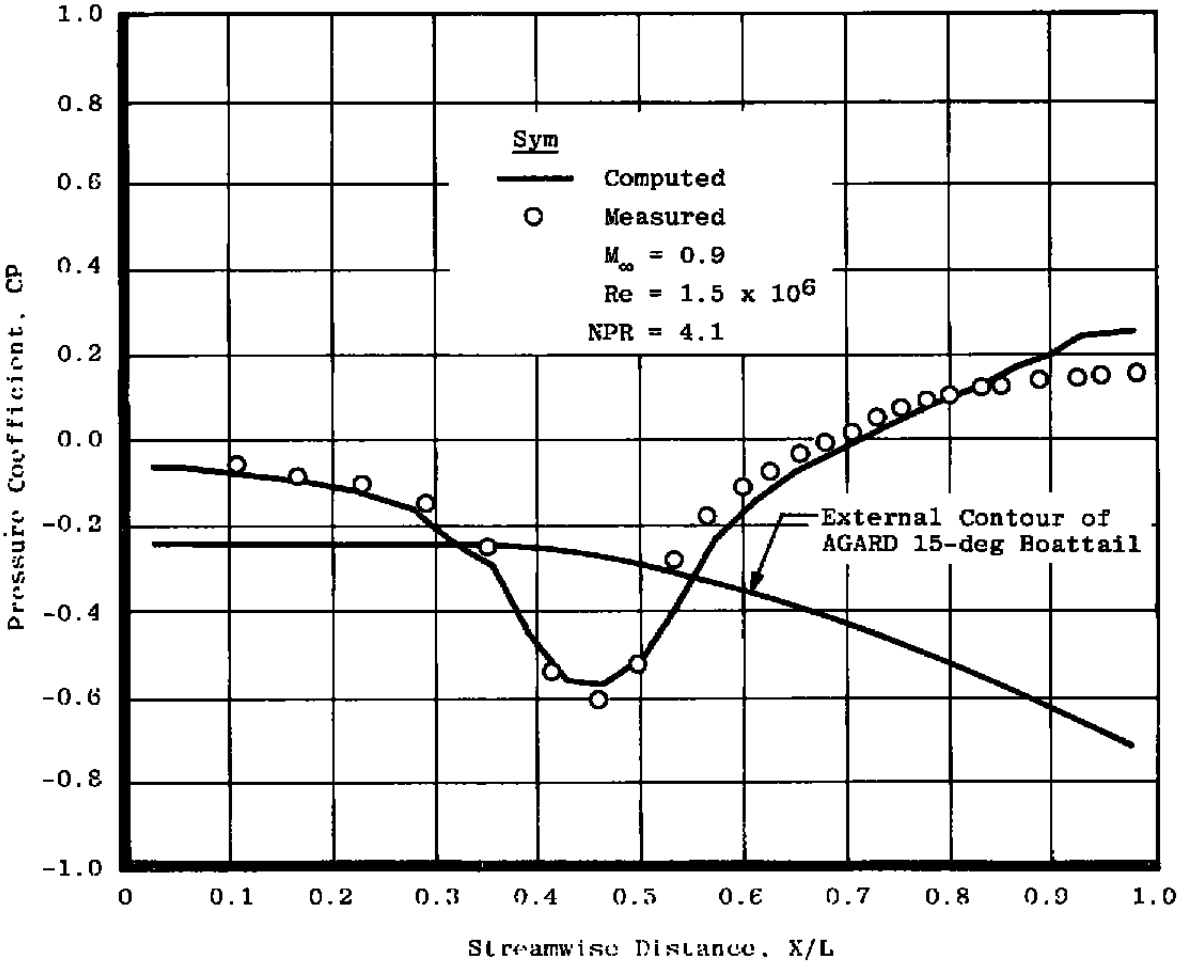

Figure 4. Computational and experimental pressure distributions for axisymmetric Navier-Stokes calculations.

this investigation demonstrated the utility and capability of a Navier-Stokes code for the study of the nozzle afterbody problem.

The high cost of computer resources required for CFD solutions makes it desirable to investigate the possibilities of using the most simplified equations available that will correctly predict the flow field of the particular problem under study. The purpose of this project was to determine the feasibility of using a viscid/inviscid interaction code to compute three-dimensional nozzle afterbody flow fields. It was believed that some of the shortcomings of previous attempts at solving this problem might be attributed to use of potential flow for the inviscid calculations, solid plume simulators that do not account for jet mixing, or direct integral boundary layers that do not allow flow separation. The code developed during this investigation, hereafter referred to as ARO2P, solves the Euler equations for nozzle afterbody

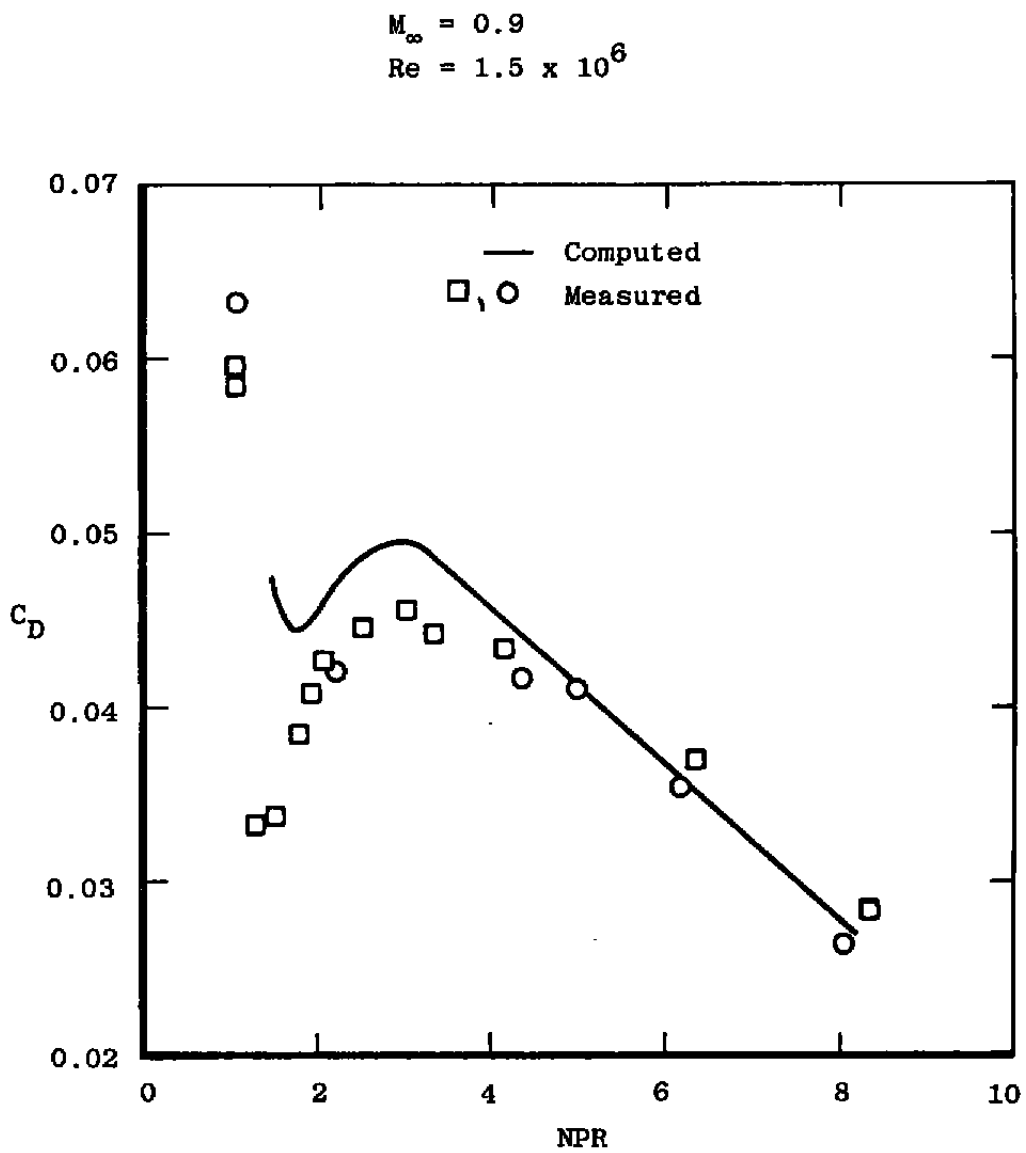

Figure 5. Effect of nozzle pressure ratio on integrated drag for axisymmetric Navier-Stokes calculations.

flow fields and the real jet plume and uses an inverse boundary-layer method for the viscid correction.

A nominal value of the measurement uncertainty of nozzle afterbody data is about five aircraft drag counts (Ref. 7). Experience has indicated that one can expect better repeatability than five counts for data obtained by pressure integration and possibly greater than five counts for data obtained with a force and moment balance. Five aircraft drag counts on a typical

$M_\infty = 0.9$

$Re = 1.5 \times 10^6$

$A/A^* = 1.225$

$\theta_N = 5$ deg

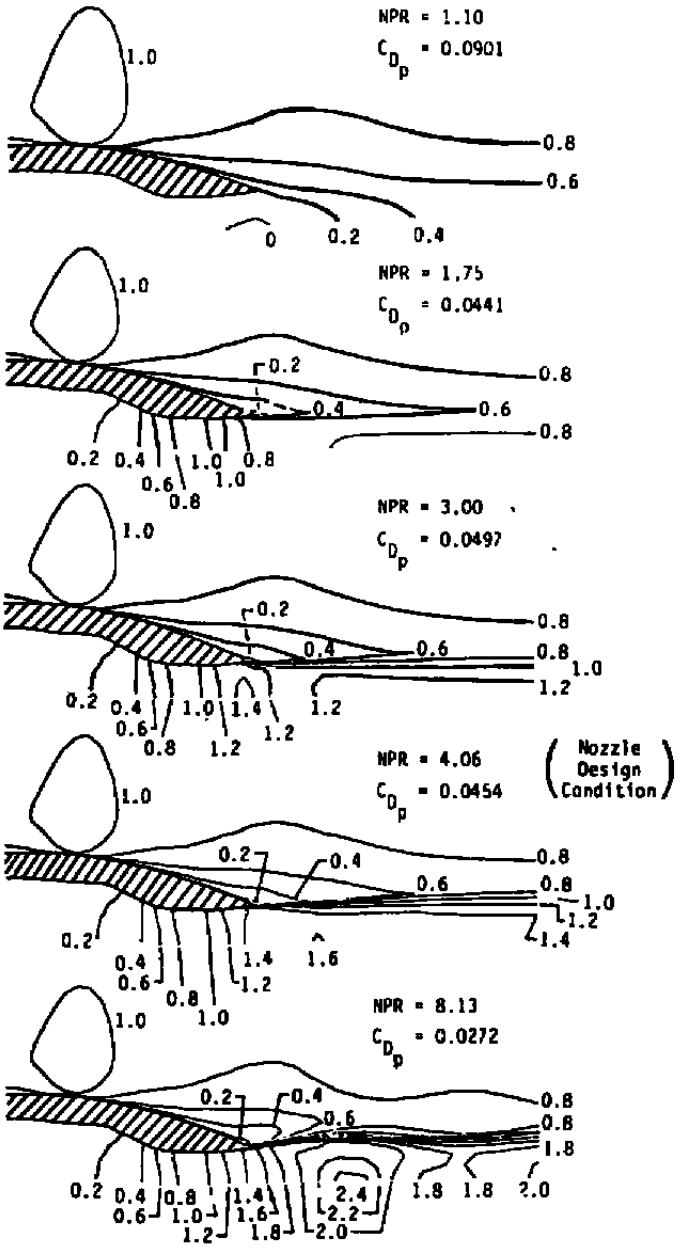

Figure 6. Mach number contours for variation in NPR for the axisymmetric Navier-Stokes calculations.

fighter aircraft is comparable to approximately 75 drag counts based on a body cross-sectional area such as was used in Ref. 5. If one is attempting to complement tunnel data by filling in points in a matrix or by extrapolating data by CFD analysis, the accuracy of the numerical solutions should be at least as good as the tunnel data. Therefore, the success criteria for evaluating the code capabilities are that calculations be within 75 body drag counts of the experiment. This is not to say the absolute value of the CFD solution must be within 75 body drag counts, but rather, incrementally the data should fall within a 150 drag count band about a line of the same slope as the data. If one is investigating an unknown situation, for example correcting tunnel data for some effect, then any computations that give solutions closer to the real answers are beneficial.

To determine the utility of the CFD code for nozzle afterbody analysis, a check case with known answers was used. For the aforementioned Navier-Stokes code and for the ensuing computational results, the AGARD 15-deg boattail afterbody provides a simple, but representative model with a sufficient wind tunnel database. Experimental data obtained on the AGARD afterbody were on a strut-mounted model (Fig. 1). The strut was not modeled for the Navier-Stokes calculations, nor was it included in the present computational grid. Interference from the strut no doubt had some influence on the experimental data, although the magnitude of this effect has not been computed. At a given Mach number, the effect of the strut interference on the drag variation with NPR is believed to be very small. Therefore, comparing slopes of the drag variation with NPR between the experiment and the CFD code is believed to be valid. Should the code prove capable of computing the effects of parameters varied in the experiments such as NPR, Mach number, or jet temperature for the check case, then it is reasonable to expect it to do the same for more complicated geometries. However, using the code to predict effects not verified by experiment would be subject to question.

2.0 CODE DEVELOPMENT AND ANALYSIS

2.1 ARO2P COMPONENTS

The inviscid core for ARO2P is the ARO1 code developed by Jacocks and Kneile (Ref. 8). It was created to solve the three-dimensional, unsteady Euler equations in Cartesian coordinates using a finite volume (volume flux) approach. The basic numerical algorithm is the explicit predictor-corrector scheme of MacCormack (Ref. 9). The viscous component is a boundary-layer correction routine developed by Whitfield, Swafford, and Jacocks (Ref. 10). It is an inverse boundary-layer method that calculates turbulent boundary layers with and without separation. "Inverse" refers to the technique whereby the boundary-layer displacement thickness is prescribed, as opposed to the direct method of calculation in which the pressure distribution is prescribed. The effect of the boundary layer is represented in the inviscid code by a transpiration condition at the appropriate boundaries.

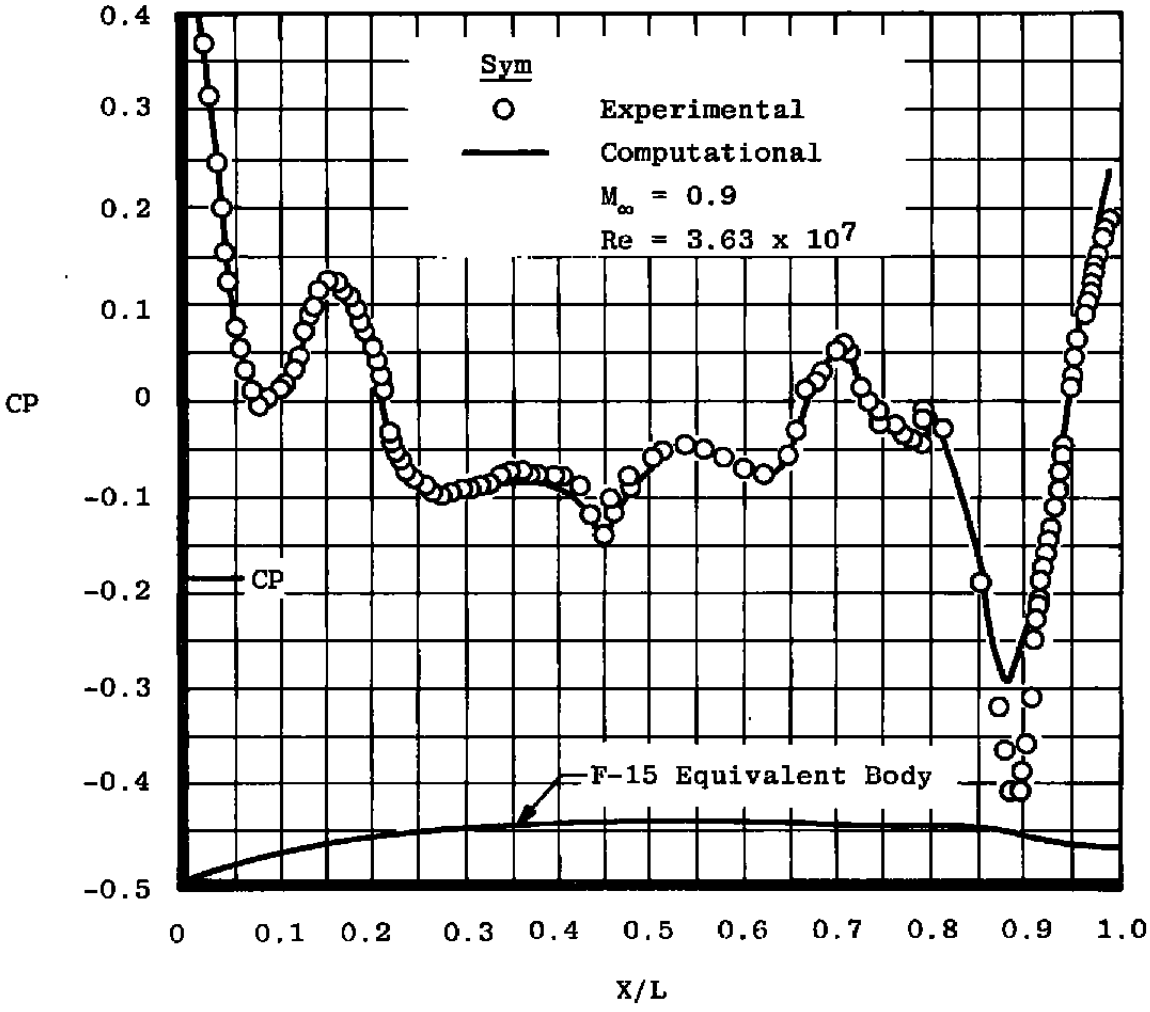

Figure 7. Computational and experimental pressure distributions for axisymmetric Euler, viscid/inviscid calculations.

Calculations were made to verify the capability of ARO2P prior to addition of the exhaust jet. Figure 7 shows the variation in pressure distribution over an F-15 equivalent body of revolution. The solutions were generated with the code operating in the viscid/inviscid mode. As with the experimental model, a solid sting was included in the calculations; there is no jet flow. The variation of pressure coefficient is in good agreement with the measured values.

The code was completed by the addition of a jet plume calculation to the inviscid routine. The jet exhaust model is based on conical flow and allows variation in NPR, temperature

ratio, nozzle area ratio, and nozzle exit angle. The addition of the plume caused a significant instability in the flow field calculation at the trailing edge of the afterbody where the free-stream and jet exhaust flow meet. To stabilize the calculations a new smoothing scheme developed by J. L. Jacocks and K. C. Reddy was integrated into the program. The routine is based on a total variation diminishing technique originated by Stephen Davis (Ref. 11).

2.2 COMPUTATIONAL GRID

The computational grids used in CFD are, in general, problem unique, varying with model geometry to adequately distribute points to resolve expected gradients. However, one can consistently use the same type of grid for the same type of problem. In fact, it is desirable to do so if the information generated by the different calculations will be used together for comparison analysis.

The type of grid chosen for ARO2P is a single piece mesh with a sectioned plume. Figure 8 depicts the transition of the grid from the computational plane to the physical plane. The top drawing shows the computational plane with two distinct sections outlined. The larger contains the free-stream flow and the smaller section the jet plume flow. The transition of the free-stream flow regime to the physical plane shows little change, but the plume section is rotated 90-deg clockwise, moved underneath the free-stream grid, and overlapped one grid line. Boundary conditions are applied over the overlapped row of the plume grid to provide a transparent connection between the plume and free-stream grid sections. Also shown in Fig. 8 are representations of the boundary conditions in the physical plane associated with each of the mesh boundaries. The top boundary is specified to simulate a porous wind tunnel wall. Other conditions represented are: free-stream and jet exhaust inflow, downstream outflow, a solid wall for the model surface modified by boundary-layer transpiration, and a reflection plane at the plume centerline. Inital conditions are uniform flow at a specified free-stream Mach number and a boundary-layer displacement thickness distribution corresponding to a cylindrical afterbody at a specified Reynolds number. Calculations were initiated 26.5 in. from the base of the model, which is approximately 10 in. upstream of the boattail region. Initial boundary-layer displacement thicknesses at the beginning of the calculation were 0.19 in. and 0.17 in. for Mach numbers 0.6 and 0.9, respectively. Figure 9 shows the physical plane mesh used for the AGARD 15-deg boattail. Notice the coarseness of the mesh in the vertical direction compared to the Navier-Stokes code mesh presented in Fig. 3. Since the Euler equations do not have the viscosity terms, no boundary layer is calculated. Therefore, there is no requirement for a dense grid at the surface to resolve the boundary-layer gradients. The boundary layers used with the inviscid codes such as ARO2P merely provide a correction to the boundary conditions specified on the body surface, but no boundary layer is calculated as part of the flow field.

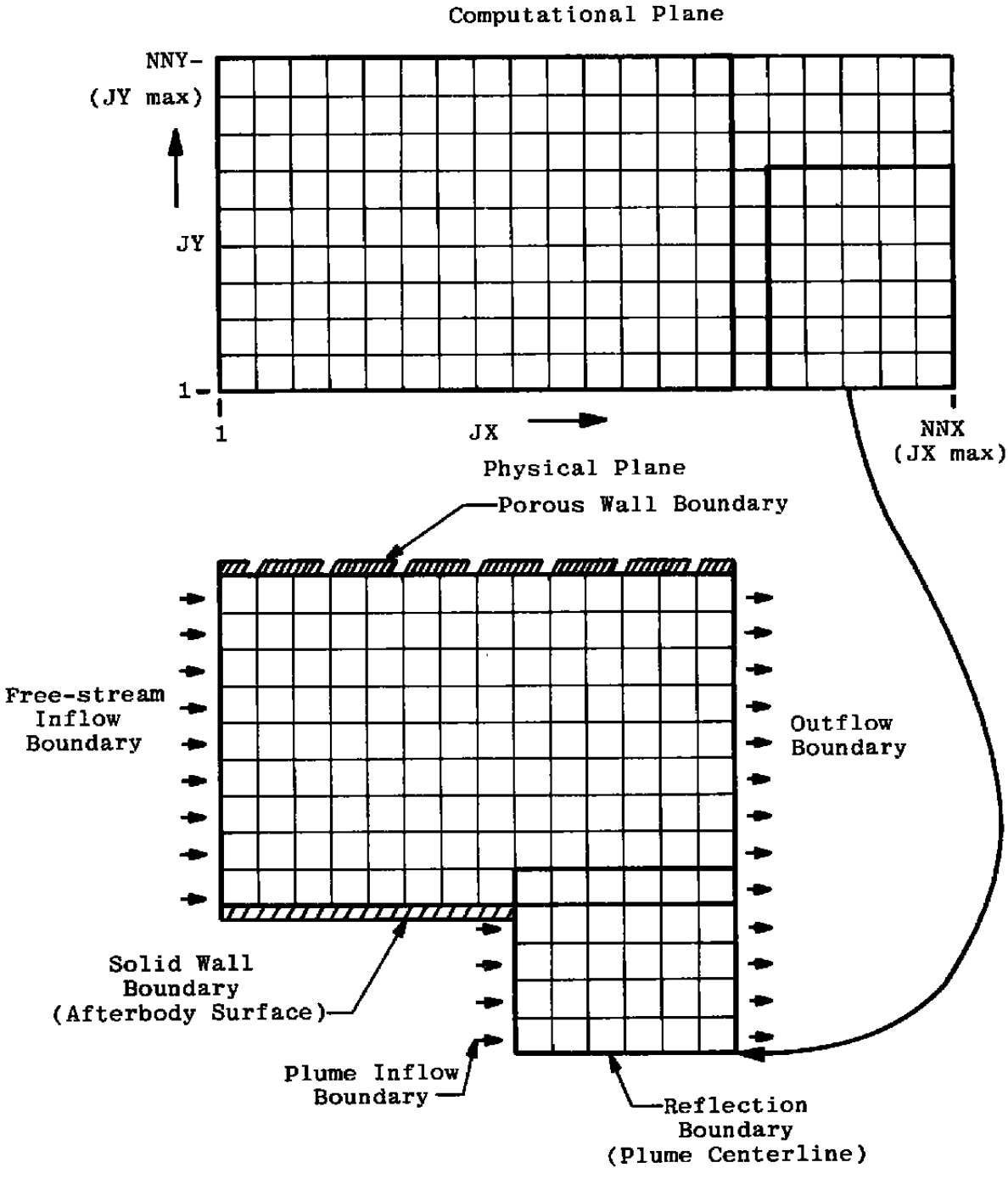

Figure 8. Transformation of the Euler code grid from the computational plane to the physical plane, in the X-Y plane.

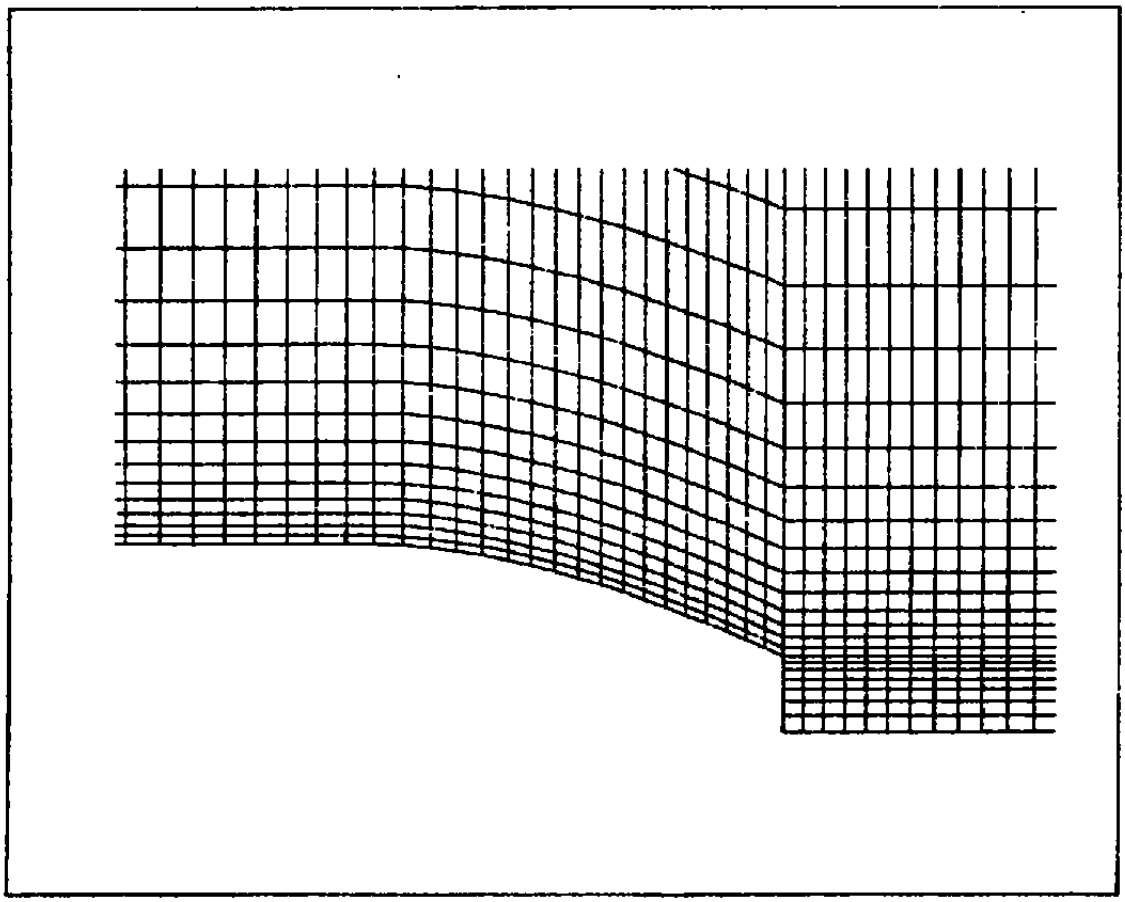

Figure 9. Euler code computation grid, physical plane.

2.3 CODE VALIDATION

Calculations were made of the flow field about the AGARD body using ARO2P with the boundary-layer calculation disabled, that is, inviscid. Figure 10 shows the variation in pressure distribution over the afterbody at the design NPR condition and a free-stream Mach number of 0.6. The computed distribution predicts a lower minimum and a higher maximum pressure, indicating that the calculation senses the actual afterbody shape with no distortion from viscous effects. Further calculations were made over a range of NPR's. A comparison of the integrated drag from the solutions with experiment is presented in Fig. 11. The slope of the inviscid calculations is in the right direction but is greater than that of the measured data. One would expect a difference in slopes in that direction considering there are no viscous effects in the calculations. Considering the previously defined accuracy requirements, the predictions do provide information concerning the direction of the integrated drag variation

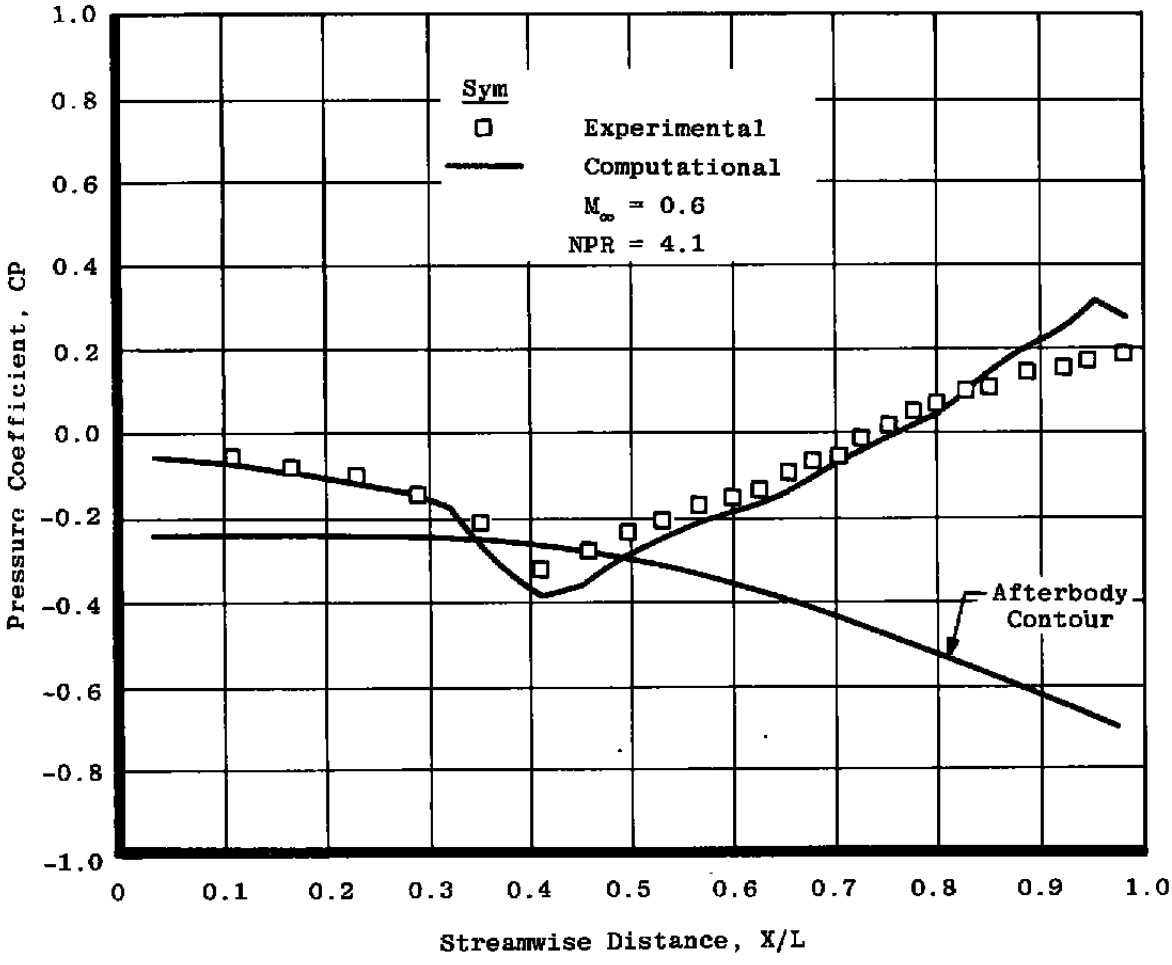

Figure 10. Inviscid pressure distribution from Euler code at design NPR.

with NPR, but they are not within a 150 drag count band for the NPR range under study. Thus, a viscous correction is required to make ARO2P useful for nozzle afterbody analysis.

There are many variables in CFD codes that affect the solution, yet have no physical meaning with respect to a real flow field. Three such variables that are used to "fine tune" the ARO2P code are: (1) the Courant-Friedrich-Lewy stability criterion (CFL number) that determines the speed with which the numerical solution progresses, (2) OMEGA - a parameter that affects the amount of smoothing applied to the flow field, and (3) NV - the number of inviscid iterations between boundary-layer corrections.

The CFL number can vary between zero and one, where one represents the maximum time stepping speed. Several solutions were calculated over the CFL range for Mach 0.6 and design NPR to determine the best stability condition. Figure 12 shows the variation of pressure

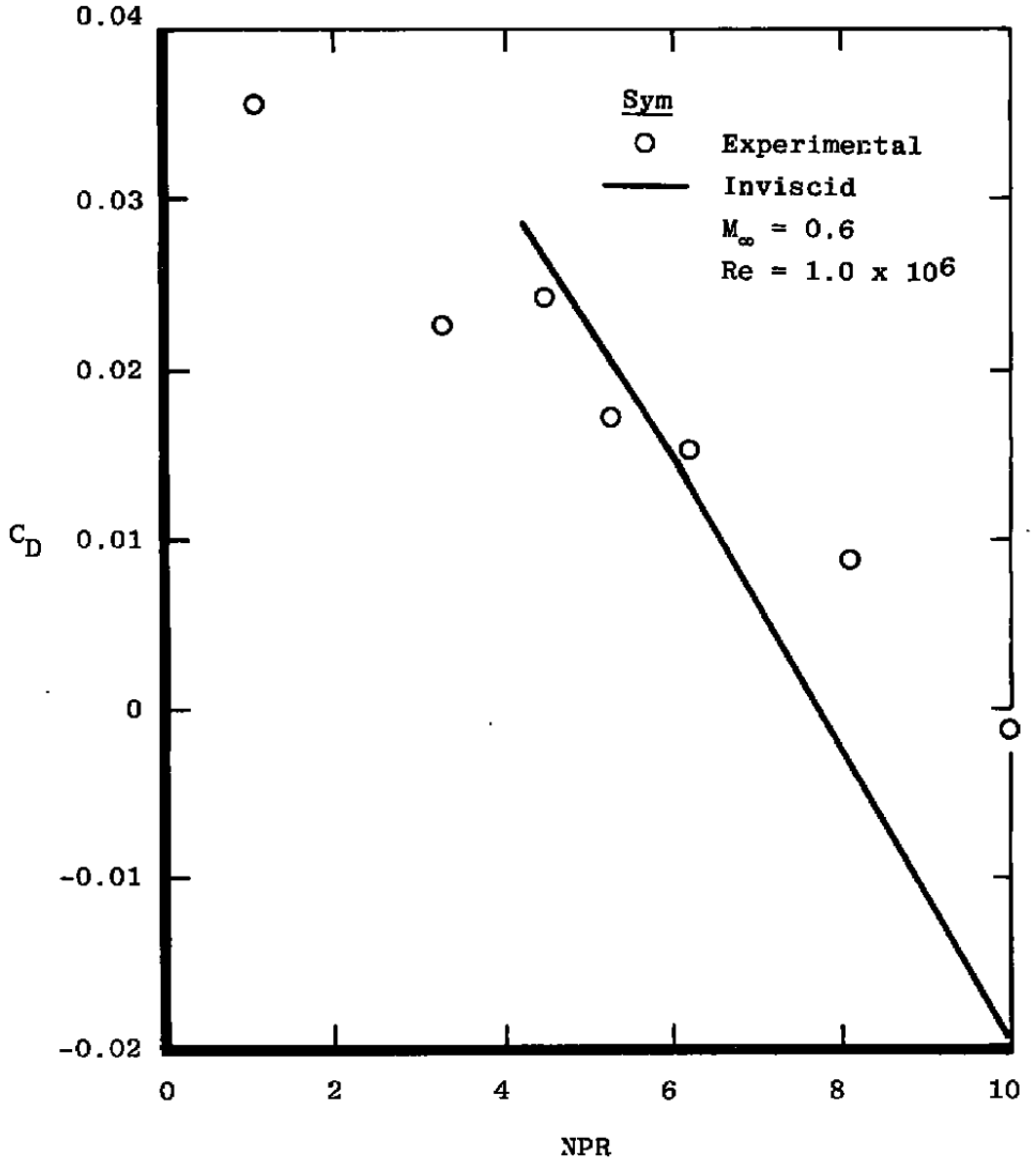

Figure 11. Experimental and computational variation of NPR with afterbody drag for the inviscid Euler code.

distribution for two of the solutions, CFL = 0.6 and CFL = 0.9. CFL = 0.6 produced the most stable solution and was thus used throughout the rest of the investigation.

A value of zero for the smoothing parameter OMEGA represents the maximum amount of smoothing available, while any number greater than zero is a decrease in smoothing. It is desirable to use as little smoothing as possible in that smoothing introduces error into the solution. Figure 13 presents the variation in pressure distribution for two values of OMEGA,

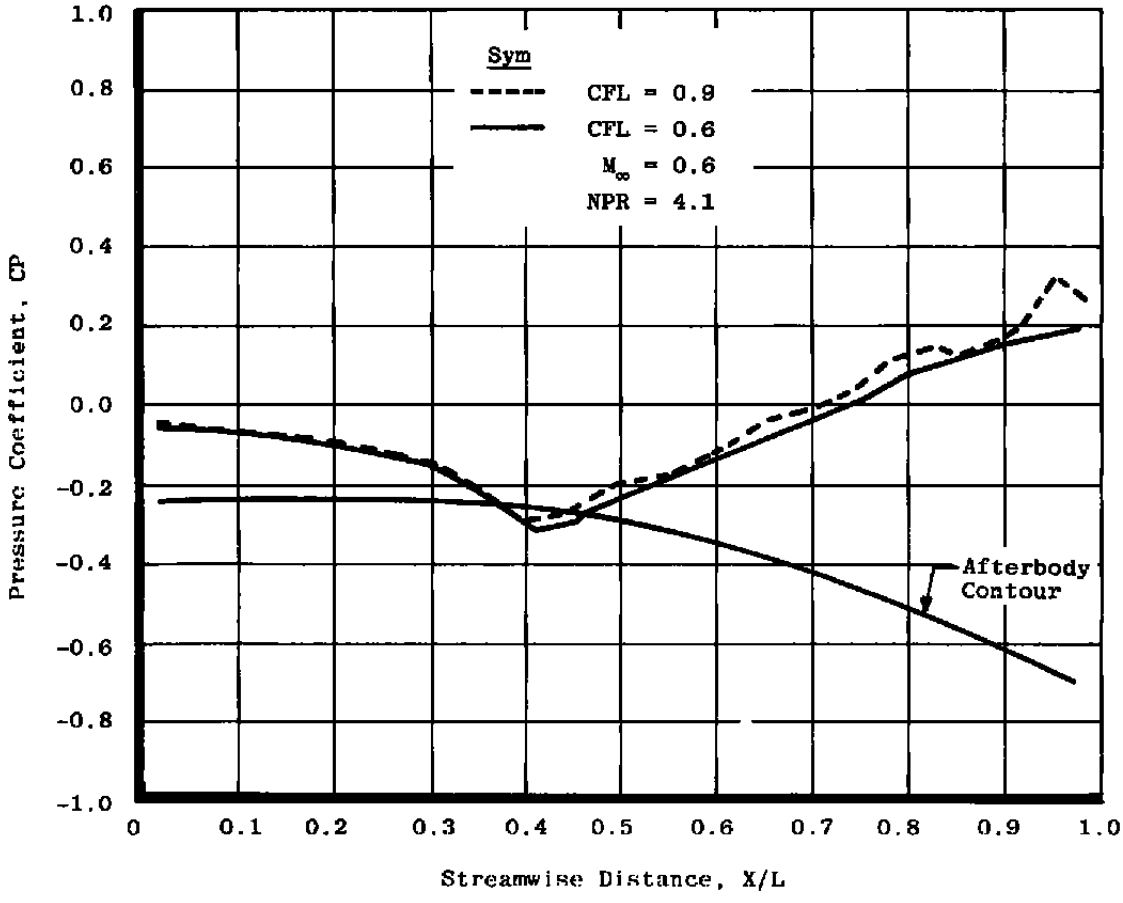

Figure 12. Variation of pressure distribution with the CFL stability criterion.

zero and one. (For reference, an OMEGA as high as four is not uncommon for other problems.) It is obvious that OMEGA = 0 produces a solution closer to the experimental data. The result was not unexpected considering the instabilities encountered earlier with the trailing edge. Consequently, the maximum smoothing available, OMEGA = 0, was used for all subsequent calculations.

Correcting the inviscid solution for viscous effects on each iteration would be very time consuming. Fortunately, it is not required. Typically, the inviscid part of a code such as ARO2P is run for a set number of iterations (NV) and then receives information for a viscous correction to its boundary conditions from a boundary-layer routine. The code is run inviscidly for NV time steps again, and another viscous correction is made based on the latest inviscid solution and so forth. Solutions were calculated with ARO2P at Mach 0.6 and design NPR for various NV's. Figure 14 shows solutions for NV = 40 and NV = 80. The difference between the two pressure distributions is minimal, although NV = 40 does appear to be slightly more stable. Therefore, NV = 40 was chosen for the rest of this analysis.

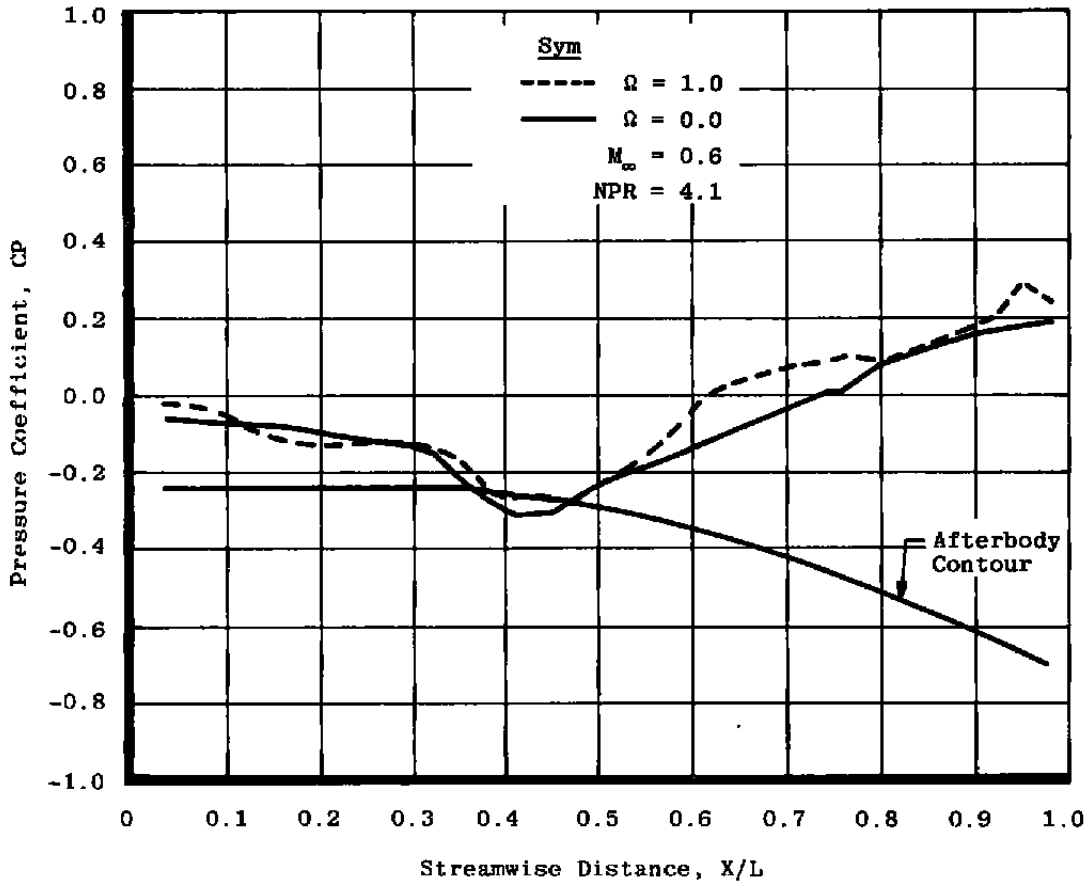

Figure 13. Variation of pressure distribution with smoothing parameter, Ω.

Figure 15 presents the data shown in Fig. 13 with the viscid/inviscid solutions. Again, the calculated values show a decrease in C_D with increasing NPR. However, rather than duplicating the slope of the experimental data, the slope of the viscid/inviscid calculations unexpectedly is steeper than the inviscid calculations. Three areas were identified that might cause such a problem: (1) errors in application of the boundary conditions, (2) application of the boundary-layer routine outside the region of its empirical correlations, or (3) the viscous mixing between the plume and free stream not being adequately simulated by the inviscid numerical viscosity.

The boundary conditions used are those presented in Fig. 8. The correctness of the application of each was verified. Contour plots were generated to ensure transparency at the overlapping boundaries of the two grid sections. The inverse boundary-layer routine in ARO2P includes empirical correlations. The correlations were not developed from nozzle afterbody data, although there is no reason to believe that they are not applicable. The effort required to investigate and/or expand the correlations is beyond the scope of the present effort.

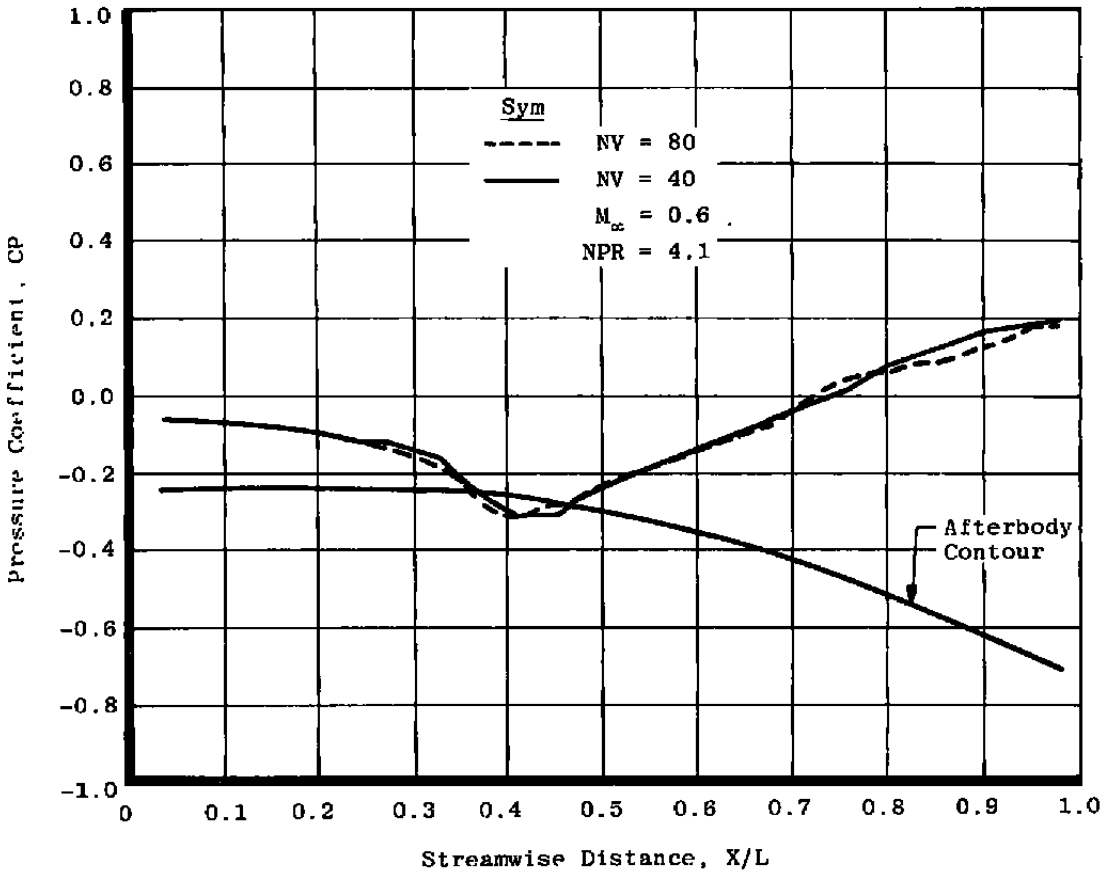

Figure 14. Variation of pressure distribution with number of time steps per boundary-layer call (NV).

There are many ways to approach the plume mixing problem. For this investigation, a major objective was to keep the correction logistically simple, i.e., avoid methods that require the mesh to change with free-stream or jet conditions, and be applicable to a wide range of nozzle afterbody problems with little modification. The approach dictated that the correction be applied along the boundary where the two grid sections meet (Fig. 8). The obvious parameter to use as a correction for plume mixing in ARO2P is ρv (density × velocity, normalized by free-stream density), which is the parameter used to correct for the viscous effects along the body. Initially, a uniform distribution of ρv along the plume boundary was used. To determine what values of ρv would be required to predict the correct variation of drag with NPR, solutions were calculated to produce pressure distributions which yielded the same integrated drag values as available experimental data. Figure 16 presents the calculated and measured pressure distributions at Mach number 0.6 and design NPR of 4.1. Albeit probably

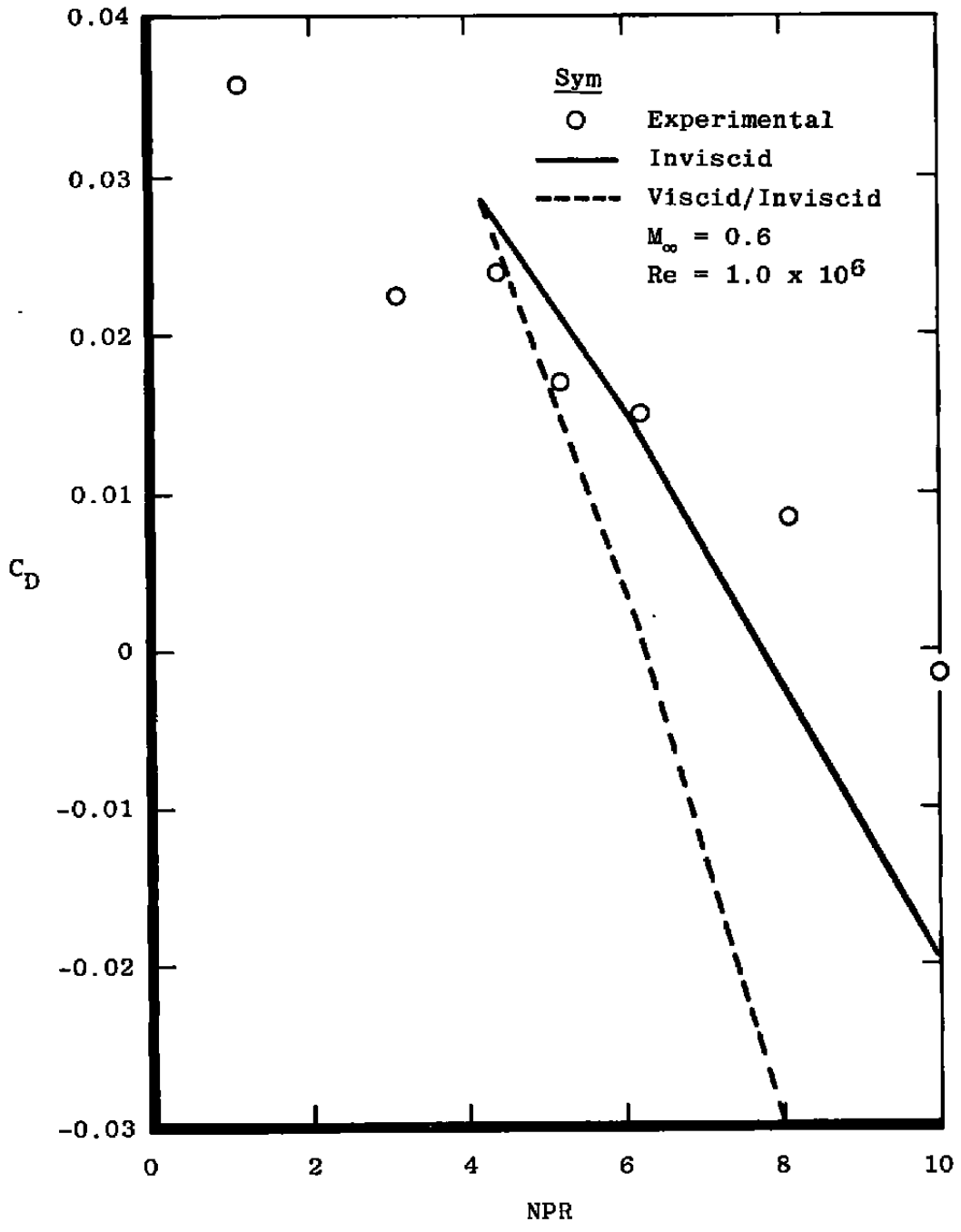

Figure 15. Experimental and computational variation of NPR with afterbody drag for the inviscid and viscid/inviscid Euler code.

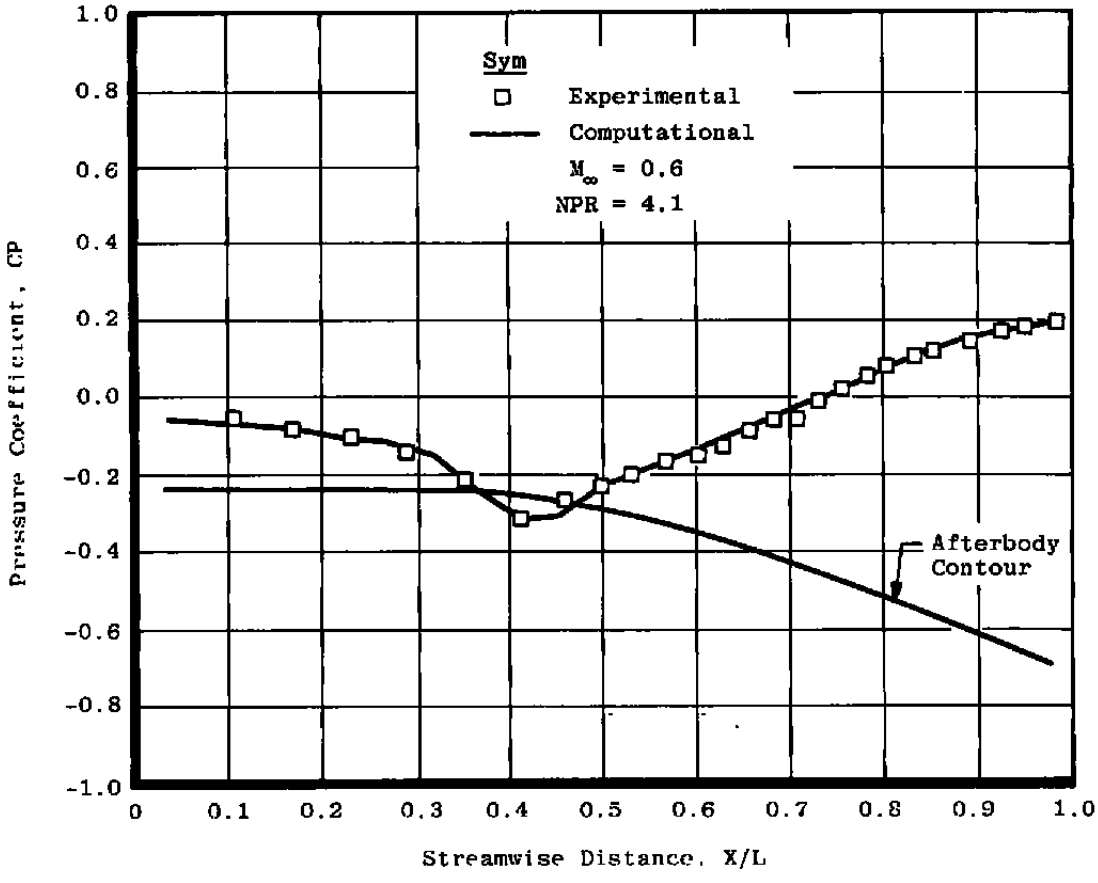

Figure 16. Experimental versus computational pressure distribution at design NPR.

fortuitous, this solution requires no correction. Figure 17 shows the results at an NPR of 10.0. The solid line shows the calculated CP distribution with no mixing correction. The dashed line was calculated utilizing a ϱv value of -1.4, which provides a satisfactory match with the data. Several Mach number 0.6 conditions were calculated for different NPR's in the same manner. The values of ϱv required to match the experimental drag data are shown as discrete data points in Fig. 18. The solid line represents a modification of the prediction technique for jet entrainment developed by Bauer (Ref. 12). Bauer's technique uses free-stream and jet exhaust conditions, including the maximum inviscid plume diameter, along with minimal geometry information to provide a coarse theoretical estimate of the induced velocity in the mixing region. The induced velocity is then used to make a first-order estimate of the effect of jet mixing on afterbody drag. The modification was produced by converting Bauer's method to a density × velocity term such as used in ARO2P. The increment of ϱv values, taken over the desired NPR range, was then scaled to match the range of the ARO2P solutions and produced the rather good correlation shown in Fig. 18. Utilizing the modified

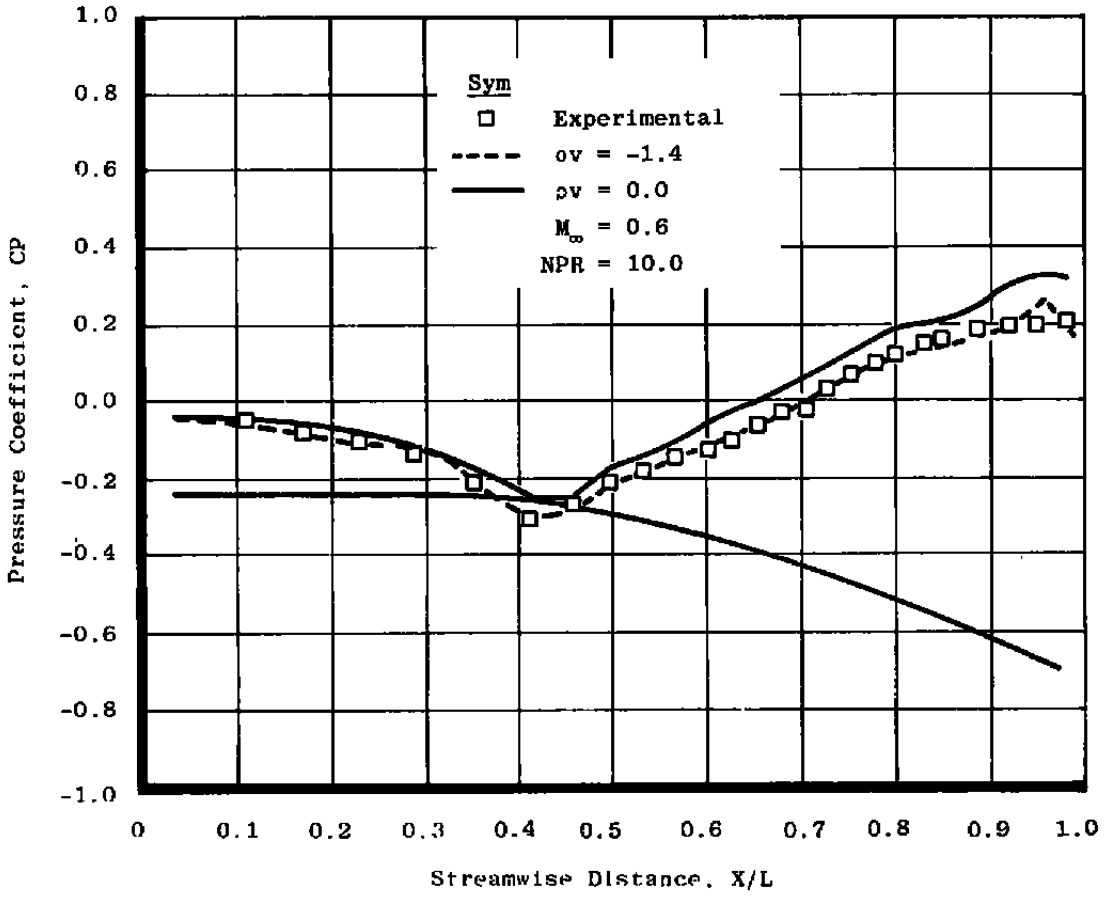

Figure 17. Variation of pressure distribution with plume mixing.

Bauer method, a prediction was made of the required ϱv values to simulate jet entrainment at Mach number 0.9 shown by the upper solid line in Fig. 18. ARO2P calculations made to evaluate the predictions for Mach 0.9 are presented in Figs. 19 and 20. The result of using the predicted ϱv value from the modified Bauer theory is shown as the dashed line on each plot; obviously, the theory is unsatisfactory. The solid lines were obtained by increasing the ϱv terms to obtain a more reasonable match to the experimental data. Even with the higher ϱv values the comparison is only marginally satisfactory, although the integrated drag values are the same. Figure 21 shows the values of ϱv required in ARO2P to match the Mach number 0.9 drag. The Bauer theory predicts smaller values of ϱv for Mach number 0.9 than for Mach number 0.6, when in reality much larger values of ϱv are required to produce marginal agreement with experiment.

Past performance of the inviscid routine from ARO2P has shown that given the right boundary-layer correction, it can calculate the correct pressure distribution, as presented in

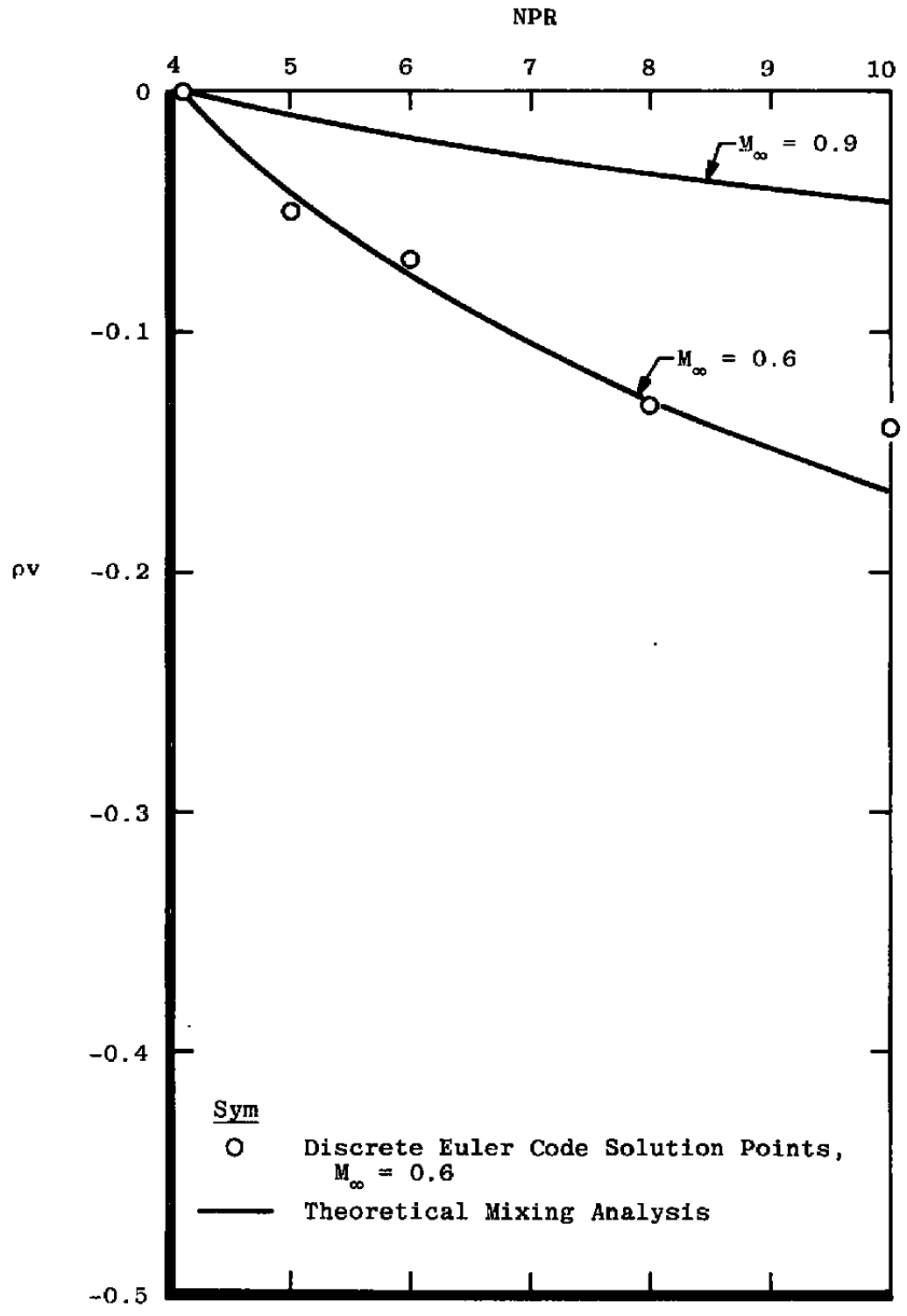

Figure 18. M_∞ = 0.6 mixing correlation and M_∞ = 0.9 mixing prediction.

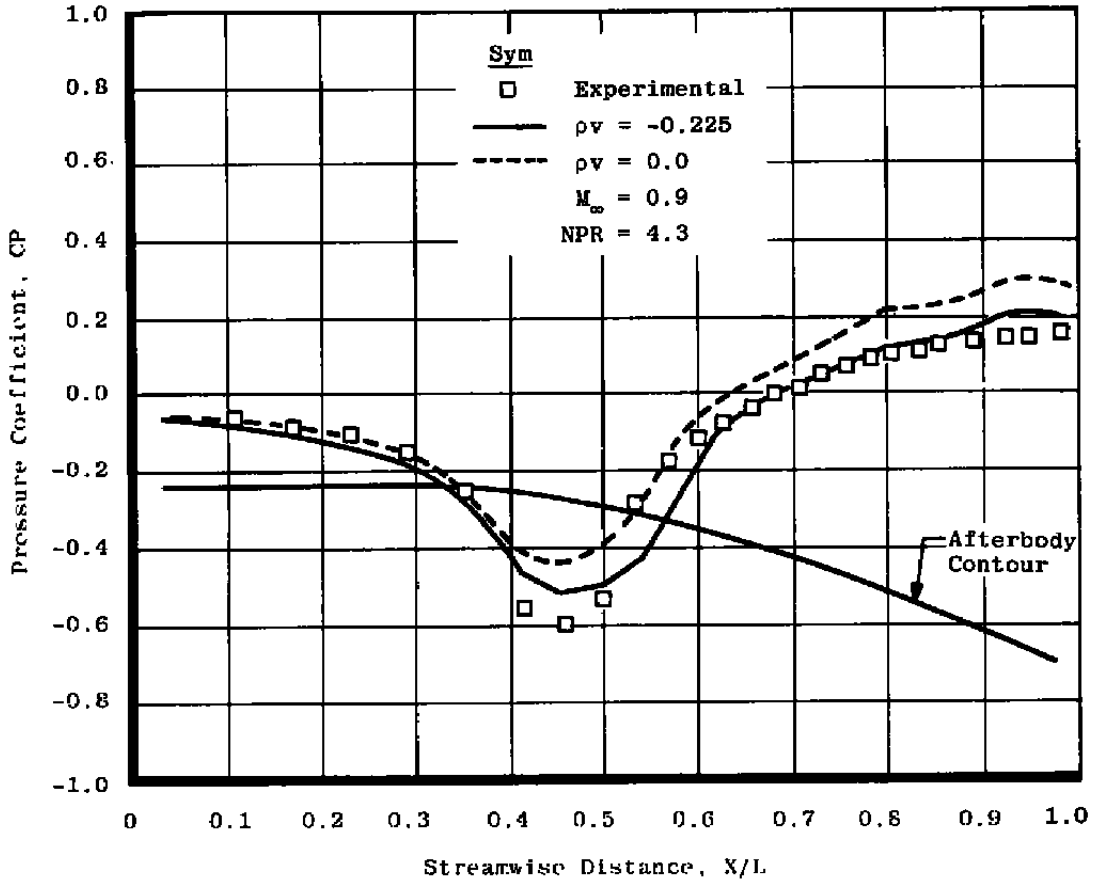

Figure 19. Variation of pressure distribution with plume mixing.

Fig. 7. Therefore, ARO2P's inability to compute satisfactory pressure distributions on the AGARD 15-deg boattail afterbody at Mach number 0.9, even with the large values of ϱv, indicates the boundary-layer simulation is not correct for this application; however, it is not apparent if the problem is caused by applying the boundary-layer routine outside its correlation range or if the mixing region between the plume and free stream is not modeled properly. The manner in which the code misses the minimum pressures as shown in Figs. 19 and 20 is the result of a too thick boundary layer in that region. Figure 22 shows the result of arbitrarily halving the boundary-layer correction. The slope of the recompression region looks better, as does the minimum pressure, but overall the comparison is worse. If the difficulty is in the boundary-layer routine, it is not uniform.

The possibility also exists that the input information provided to the boundary-layer routine by the inviscid portion of the code is incorrect because of poor simulation of the mixing process. Calculations were made to investigate the effect of the shape of the ϱv distribution

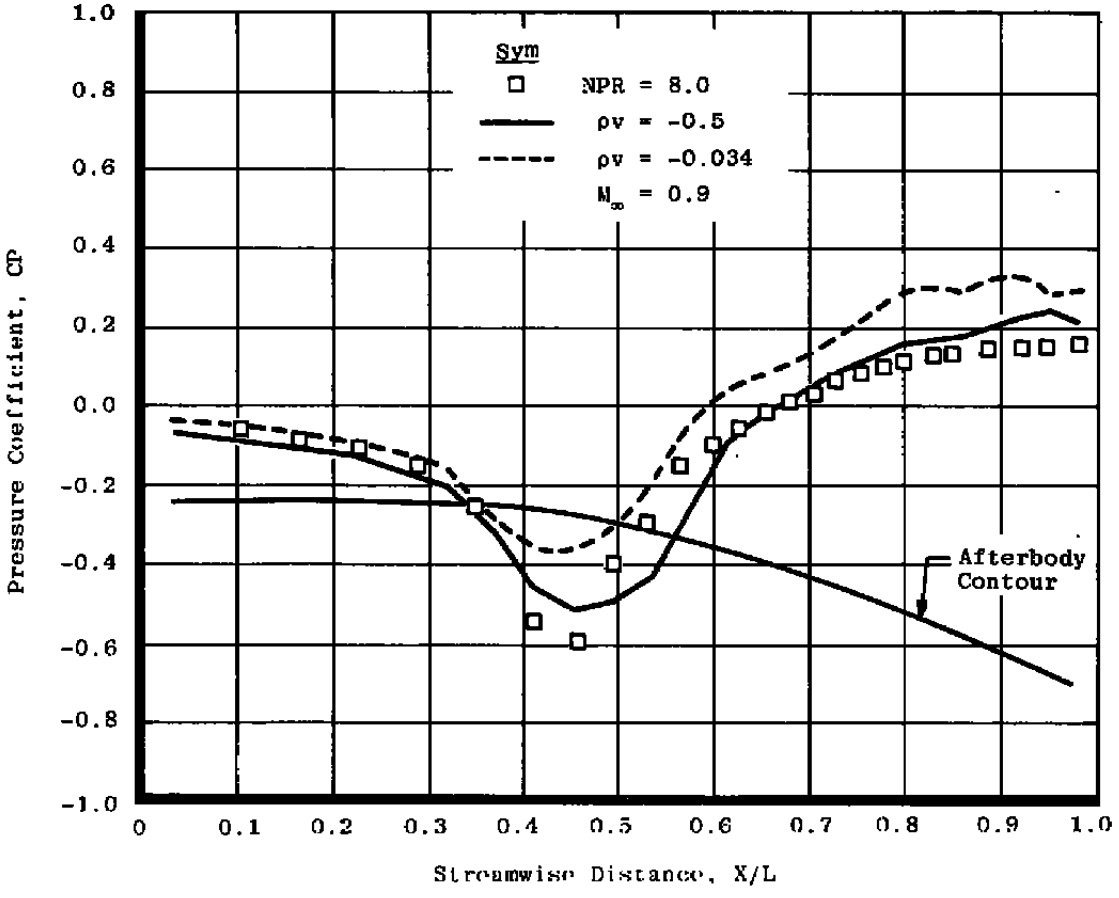

Figure 20. Variation of pressure distribution with plume mixing.

being applied along the plume grid boundary. Figure 23 presents the variation in pressure distribution for two modifications of the ϱv distribution. The tapered distributions were applied along the plume grid boundary from the trailing edge to a point downstream of the maximum plume diameter, as calculated by the method of characteristics. Applying the modified ϱv distributions does not produce the desired pressure distribution.

Although the code calculates excellent afterbody pressure distributions with a solid plume simulator, as presented in Fig. 7, the addition of the plume and boundary layer to the calculations did not produce the desired results. The calculated variation of drag with NPR is in the right direction but the magnitudes are not satisfactory. Attempts to model the jet mixing in the inviscid code with a simple theory failed to adequately correct the problem so that the code could make useful predictions. No simple modification was found to increase accuracy.

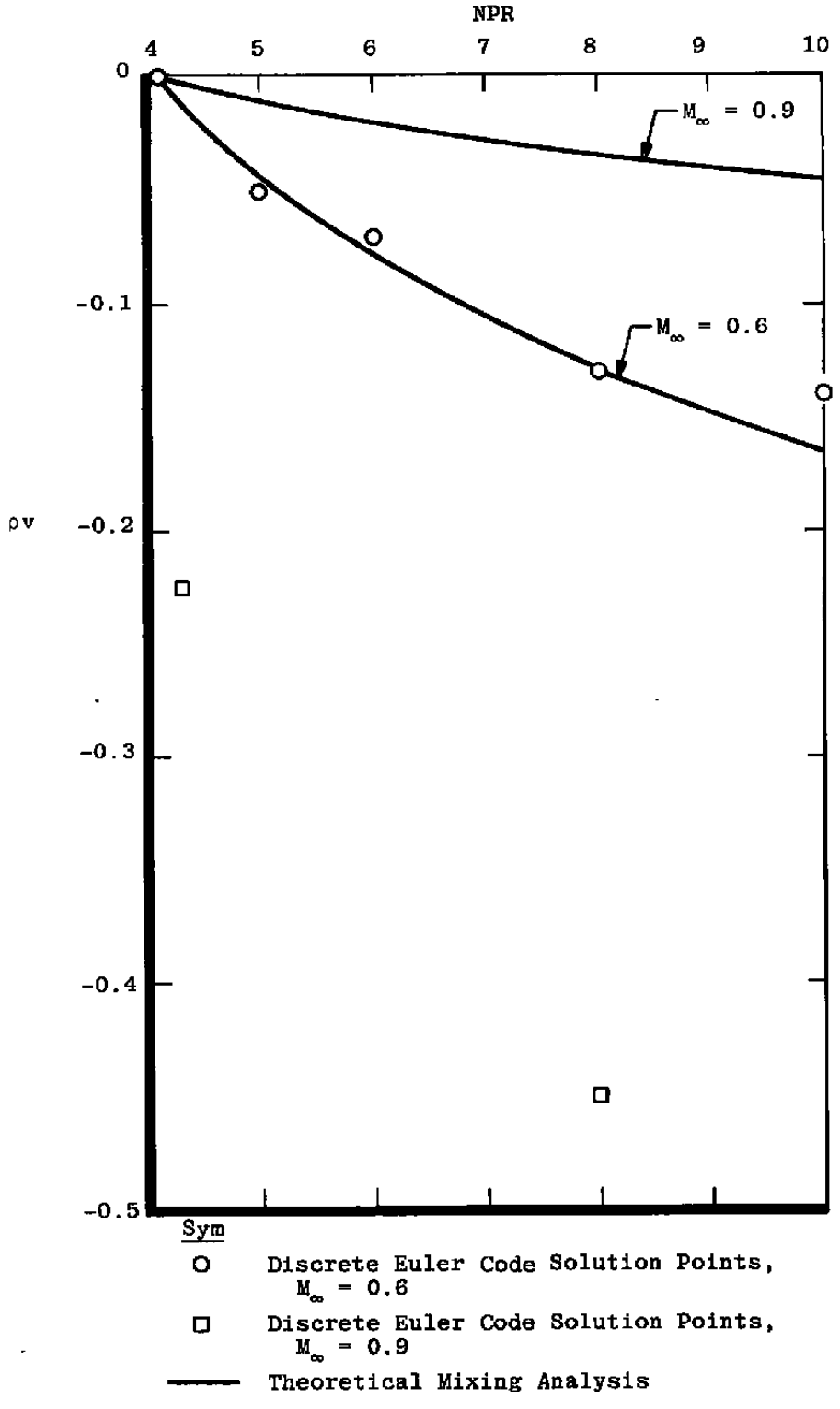

Figure 21. Mixing correlation prediction results.

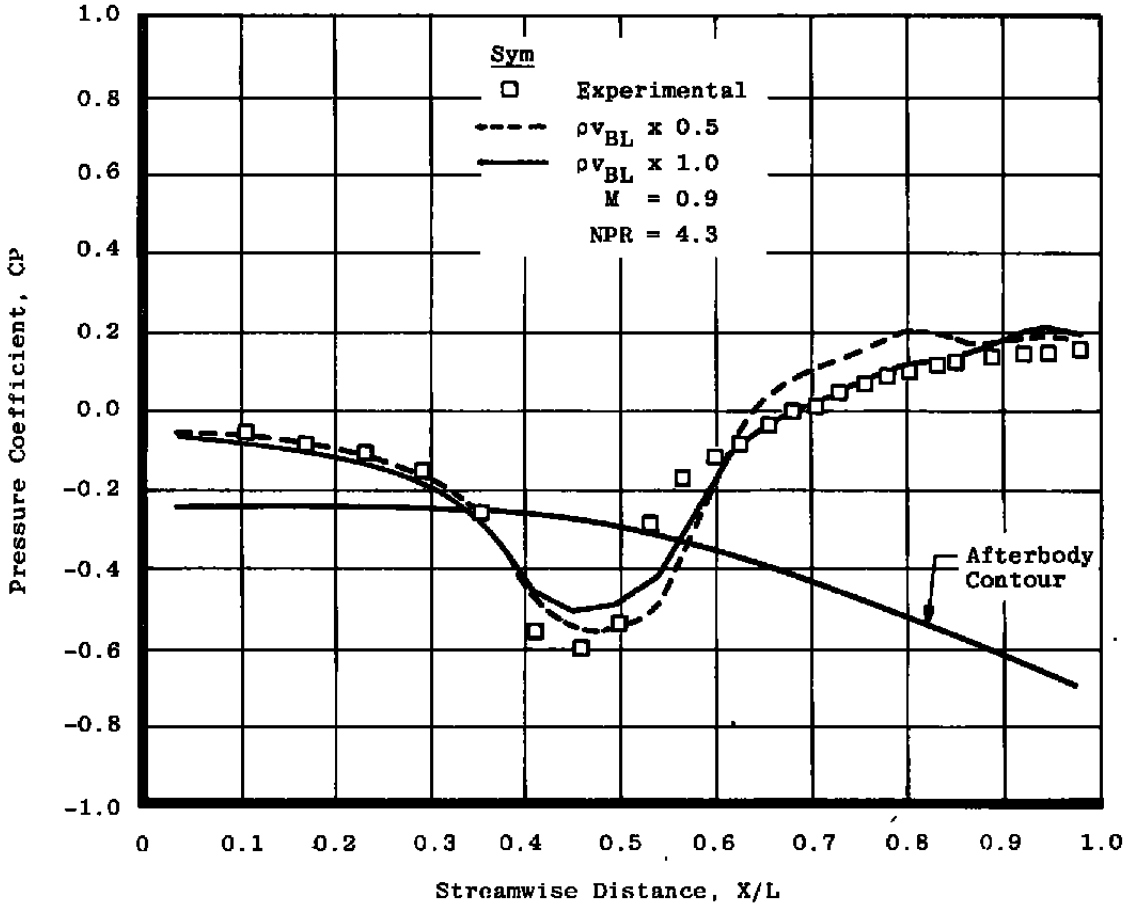

Figure 22. Pressure distributions for uniform variation in inverse boundary layer ρv predictions.

3.0 CONCLUDING REMARKS

A CFD code was developed which coupled an inverse boundary-layer routine with an Euler code incorporating a jet plume. Calculations were made on the axisymmetric AGARD 15-deg boattail afterbody for variations in NPR at Mach numbers 0.6 and 0.9, and compared to experimental results. Although the code predicted drag changes in the right direction, the accuracy was poor. An attempt was made to incorporate a relatively simple model of jet mixing, but the results indicated that a more in-depth understanding of the jet mixing process is required to produce such a modification.

To satisfy the needs for a three-dimensional nozzle afterbody analysis tool within the current state of the art, it appears that a Navier-Stokes code is required. Jacocks, et al. (Ref. 4), demonstrated the capabilities of such an approach for axisymmetric flows. Successful

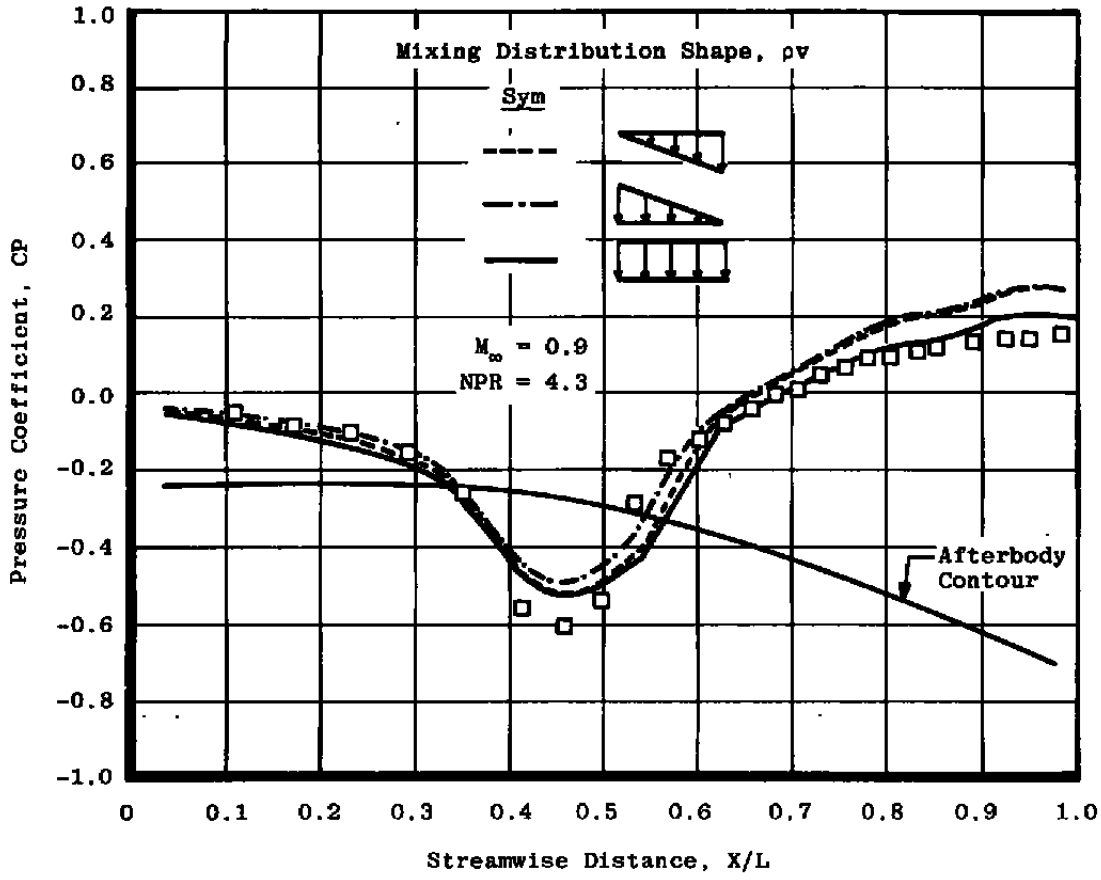

Figure 23. Variation in pressure distribution with mixing parameter distribution.

application of a Navier-Stokes code for a three-dimensional situation would be very useful in providing insights into the physics of the complex boundary-layer/plume interaction phenomena. Perhaps one can learn from such a code an acceptable means of representing the afterbody boundary layer and plume mixing, thereby allowing the use of a viscid/inviscid approach.

REFERENCES

1. Kennedy, T. L. "An Evaluation of Wind Tunnel Test Techniques for Aircraft Nozzle Afterbody Testing at Transonic Mach Numbers." AEDC-TR-80-8 (AD-A091775), November 1980.

2. Price, Earl A., Jr., "Interference on a Model Afterbody from Downstream Support Hardware at Transonic Mach Numbers." AEDC-TR-80-27 (AD-A093739), January 1981.

3. Lucas, Ernest J. "Model Size and Humidity Effects on Selected Calibration Parameters for the 16-ft Transonic Wind Tunnel at AEDC." AEDC-TR-81-17 (AD-A107728), November 1981.

4. Jacocks, J. L., Peters, W. L., and Guyton, F. C. "Comparison of Computational and Experimental Jet Effects." *Journal of Aircraft,* Vol. 19, No. 11, November 1982, pp. 963-968.

5. Jacocks, J. L. "Computation of Axisymmetric Separated Nozzle Afterbody Flow." AEDC-TR-79-71 (AD-A079694), January 1980.

6. Peters, William Lee. "An Evaluation of Jet Simulation Parameters for Nozzle Afterbody Testing at Transonic Mach Numbers." AEDC-TR-76-109 (AD-A031525), October 1976.

7. Price, Earl A., Jr. "An Investigation of F-16 Nozzle-Afterbody Forces at Transonic Mach Numbers with Emphasis on Support System Interference." AEDC-TR-79-56 (AD-A078693), December 1979.

8. Jacocks, J. L. and Kneile, K. R. "Computation of the Three-Dimensional Time-Dependent Flow Using the Euler Equations." AEDC-TR-80-49 (AD-A102463), July 1981.

9. MacCormack, R. B. "The Effect of Viscosity in Hypervelocity Impact Cratering," AIAA Paper No. 69-354, May 1969.

10. Whitfield, D. L., Swafford, T. W., and Jacocks, J. L. "Calculation of Turbulent Boundary Layers with Separation and Viscous-Inviscid Interaction." *AIAA Journal,* Vol. 19, No. 10, October 1981, pp. 1315-1322.

11. Davis, Stephen F. "TVD Finite Difference Schemes and Artificial Viscosity." NASA Contractors Report 172373, ICASE, June 1984.

12. Bauer, R. C. "A Method for Estimating Jet Entrainment Effects on Nozzle-Afterbody Drag." AEDC-TR-79-85 (AD-A080955), February 1980.

NOMENCLATURE

A/A^*	Nozzle exit area-to-throat area ratio
C_D	Afterbody drag coefficient based on pressure integrations
CFL	Courant-Friedrich-Lewy number
CP	Afterbody surface pressure coefficient
M_∞	Free-stream Mach number
NPR	Nozzle total pressure to free-stream static pressure ratio
NV	The number of inviscid iterations between boundary-layer corrections
OMEGA or Ω	Smoothing parameter
R	Body radius
Re	Free-stream Reynolds number, per foot
v	Velocity in y-direction
x,y,z	Cartesian coordinates
X/L	Nondimensionalized body length
θ_N	Nozzle divergence half-angle, deg
ϱ	Density